PROCEEDINGS, 48th Workshop on Geothermal Reservoir Engineering
Stanford University, Stanford, California, February 6-8, 2023
SGP-TR-224

Long-term Temperature Monitoring of a Campus-Scale Geothermal Exchange Field using a Fiber-Optic Sensing Array

Shubham Dutt Attri[1], Evan Heeg[2], Mehmet Yilmaz[3], James M. Tinjum[4], Dante Fratta[5], David Hart[6]

[1]Graduate Student, Industrial and Systems Engineering, University of Wisconsin-Madison, Madison, WI, USA, sattri@wisc.edu,

[2]Graduate Student, Geological Engineering, University of Wisconsin-Madison, Madison, WI, USA, epheeg@wisc.edu,

[3]Postdoctoral Research Associate, Civil and Environmental Engineering, University of Wisconsin-Madison, Madison, WI, USA,

[4]Associate Professor, Geological Engineering, Civil and Environmental Engineering, University of Wisconsin–Madison, Madison, WI, USA, email: jmtinjum@wisc.edu

[5]Associate Professor, Geological Engineering, Civil and Environmental Engineering, University of Wisconsin–Madison, Madison, WI, USA, email: fratta@wisc.edu

[6]Professor, Wisconsin Geological and Natural History Survey, University of Wisconsin–Madison, Madison, WI, USA, email: djhart@wisc.edu

Keywords: fiber optics, distributed temperature sensing, district-scale geothermal, ground heat exchange, ground-source heat pumps, data analytics

ABSTRACT

Increases in greenhouse gas (GHG) emissions and global temperature have occurred since the Industrial Revolution due to a constant increase in fossil energy consumption and emissions. Geothermal heat exchange (GHX) systems replace conventional heating and cooling methods and have higher system efficiency and decreased dependency on fossil fuels. Detailed, long-term monitoring of GHX fields is essential to improve the operation and sustainability of GHX systems. However, there is a need for more research on the long-term monitoring and performance analysis of low-temperature geothermal fields. To address this issue and evaluate a GHX system's efficiency, we collected geothermal temperature data from a large geothermal field in the Midwest. In this study, we investigate the temperature increase of a large-scale borehole field and its relationship to subsurface properties and we assessed errors and noise in the long-term temperature data. We have used fiber-optic (FO) distributed temperature sensing (DTS) for over seven years to monitor the performance of a 280-m by 360-m, 2596-borehole GHX field, to quantify the role of groundwater flow, and to evaluate the distributed thermophysical properties on subsurface heat transfer and storage. Like most GHX systems in the US, this field is subjected to cooling-dominated loads; likewise, the data show a gradual increase in subsurface temperature over the past seven years. However, high-frequency fluctuations in long-term temperature measurements are of concern. We worked to identify the sources of those fluctuations by analyzing potential errors and noise in the calibration formulation, the bath temperature measurements, and the raw data the interrogator gave. Better control over long-term noise in the data may be used to improve design approaches, develop more robust energy balance assessment formulation, and implement long-term ground temperature change models.

1. INTRODUCTION

1.1 Fiber-optic distributed temperature sensing

Fiber-optic (FO) distributed temperature sensing (DTS) is an approach that uses Raman spectra scattering of laser light pulses in a fiber optic cable to provide real-time spatial and temporal data (Suarez et al. 2011). Originally used by oil and gas industries since the late 1980s for pipeline monitoring, the DTS technique has become more popular for measuring temperatures since 2006 (Hausner et al. 2011). Modern commercially available DTS systems can measure temperature resolutions of 0.01 °C, spatial resolutions of less than 1 m, temporal resolutions of 10 s or more, and array lengths of several km. With these resolutions, sensor density, and environmental insensitivity, FO-DTS offers significant improvements over traditional electrical-based sensors (such as thermocouples and thermistors) for field temperature measurements. A DTS interrogator sends a short pulse of laser light along the fiber and backscattered photons are detected. Most of the scattering is elastic and therefore has the same frequency as the original light pulse, but some of the backscattered photons are nonelastic Raman scattering that results in light at wavelengths greater than (Stokes) and less than (anti-Stokes) the original frequency in the pulse. Anti-Stokes photons are much more sensitive to temperature than Stokes photons. Below a critical light intensity, the magnitude of both Stokes and anti-Stokes scattering varies with the intensity of the illumination. Furthermore, the anti-Stokes scattering is an exponential function of the temperature along the length of the fiber (Selker et al. 2006). So, the corrected ratio of the anti-Stokes and Stokes amplitudes of the Raman scattering is used to obtain a profile of the temperature along the length of the fiber (Suarez et al. 2011).

1.2 Ground-Source GHX Heat Pumps

A Geothermal Heat Exchange (GHX) System is a method for space conditioning and domestic hot water heating (ASHRAE 2011). In general, GHX systems are shown to be more energy-efficient and economic over time when compared to conventional space-conditioning and water heating systems, despite the energy-demanding and expensive installation process of GHX systems (Bloom and Tinjum 2016, Reddy et al. 2020). There are several GHX system configurations, including open-loop and closed-loop systems. Open-loop systems draw water directly from groundwater or a surface body of water, while closed-loop systems circulate fluid underground through high-density polyethylene (HDPE) pipe as the ground is used as a thermal reservoir. In both cases, the geothermal-conditioned water in the system

interacts with a heat pump for space conditioning and hot water heating (ASHRAE 2011). The size of these GHX systems can vary drastically as they can be installed for a single residential house, district-scale facilities, or anything in between. The design of these systems often assumes homogeneous subsurface heat transfer as to a single geologic unit, which, of course, is not always correct due to varying thermophysical properties of geological formations with depth. In addition to geology, groundwater flow also impacts heat transfer (McDaniel et al. 2018a). The ability to understand, monitor, and predict GHX performance throughout the lifetime of the system can be improved by investigating the variability of the subsurface and how it affects the long-term performance of the geothermal system. Monitoring can be further used to assess the associated environmental and working costs, and performance of the system more accurately and make better decisions for the viability and impacts of future projects. This monitoring can be done by employing FO-DTS technology throughout the system to obtain temperature data in the desired resolutions and accuracy. Furthermore, the temperature data can be analyzed over space and time to analyze and evaluate the GSHP system. There are diverse ways for deploying FO-DTS depending upon the usage, but the most important part of using the technology is the calibration methodology, which should be chosen after thorough study of the available methods and techniques.

1.3 Calibration of DTS Arrays

Fiber-optic cables can be configured as simple single-ended, duplex single-ended, and double-ended configurations as shown in Figure 1 (Hausner et al. 2011). In a single-ended installation, there is only one connection between the instrument or interrogator and the cable measuring the temperatures along its length and the fiber is calibrated using three different baths. The fiber and instrument have only one connection in the duplex single-ended system as well, but the fiber is looped along the same path, so the fiber is in calibration baths at the beginning and at the end, as shown in Figure 1b. In the double-ended calibration setup, both ends of the fiber are connected to two different channels of the interrogator (Figure 1c). In the double-ended calibration, the temperature is measured from both the ends of the fiber. In all these configurations, non-uniformities along the fiber such as damages, connections, and fusion splices affect the attenuation of the signals. The duplex and double-ended calibration can potentially correct these non-uniform attenuations along the fiber and are thus preferred whenever feasible (Hausner et al. 2011).

The calibration method used to determine the temperatures along the fiber is based on the basic physics of backscattering, and the power of stokes (P_s) and anti-stokes (P_{as}) signals are translated to the temperature at a location z (m) from the instrument using equation (1) (Van de Glesen 2012, McDaniel et al. 2018b, des Tombe 2020):

$$T(z,t) = \frac{\gamma}{ln\frac{P_S(z,t)}{P_{as}(z,t)} + C - \int_0^z \Delta\alpha \, . \, z' \, dz'} \tag{1}$$

where γ represents the shift in energy between incident and the backscattered Raman photons, C is a dimensionless constant that depends on the properties of incident LASER and the DTS instrument, and $\Delta\alpha$ (m^{-1}) is the differential attenuation between the anti-Stokes and Stokes signals in the fiber. The calibration routines depend on reference temperatures (sections of known temperature) on the cable to find these constants.

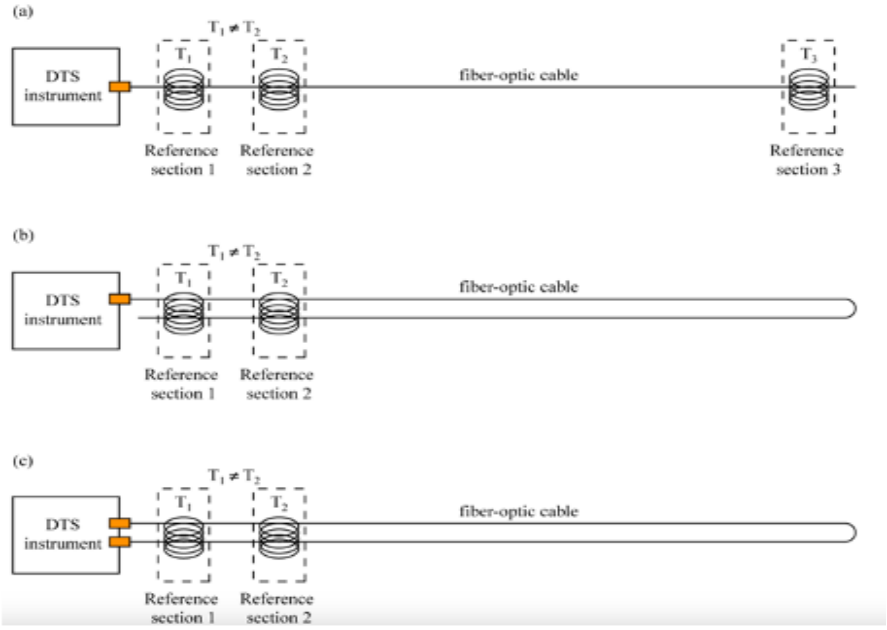

Figure 1: Fiber optic configurations for distributed temperature sensing - (a) Single-ended; (b) Duplex single-ended; (c) Double-ended (from Hausner et al. 2011)

Calibration routines involve calculating the three constants $\gamma, \Delta\alpha, and\ C$ using constant and known temperature reference points along controlled sections of the fiber. In principle, this calibration method would require temperatures of at least three spatially distinct locations

constant on the time scale. Hausner et al. (2011) described in detail the different calibration methodologies including explicit calculations, interpolation, and optimization for different scenarios to find out the constants and, thus, temperatures with varying levels of precisions. These calibrations can either be static or dynamic, based on the assumption of whether the parameters are dependent or independent of the time scale. Static calibration assumes these parameters are constant with time and derived from the initial trace to each time slice of the DTS data. However, suppose the temperature of the reference cable diverges over time from the initial temperature measured by the monitoring thermometer due to any reason, like environmental changes. In that case, the fiber-optic system will report erroneous data. Static calibration can only work in a carefully controlled environment or be used when the limited accuracy is not problematic or the outcome expected is binary, for instance, for detecting fire. For more accurate readings, dynamic calibration is required. It allows the calculation of the constants at each timestep of data collection as it relies on temperature baths to dynamically record reference temperatures and recalculate the parameters.

This study provides an example of a long-term dynamic calibration of a complex fiber-optic network buried within a low-temperature geothermal exchange borefield. The double-ended calibration methodology was used and is explained in detail. Long-term data analysis and insights are provided to allow the researchers to study the temperature changes in the field over time and its potential effects. The changes in the instrumentation setup over time, the potential reasons for error and noise in calibration, and the impact of cooling-dominated loads on the ground temperature and system efficiency are also studied. The final objective was to understand and quantify the bias in long-term temperature measurements, improving their accuracy.

2. FIELD SETUP AND INSTRUMENTATION

2.1 Field Site

The campus of a company in southern Wisconsin houses around 10,000 employees in over 19 office buildings. Due to the heat generated during daily use of the campus, the HVAC load is cooling-dominated. To be energy neutral, the campus relies on wind energy, solar energy, and four district-scale geothermal borefields with a cooling pond. The borefields have 6,172 U-pipe GHXs that provide 48.5 MW of cooling capacity and a cooling pond with 1,300 coiled loops that provide 4.2 MW of cooling for limited intervals. Borefield number 4 provides more than 50% of the capacity and it was added to control the overheating of the other fields. Aa the campus creates predominant cooling loads; the temperature in the field increases causing a decrease in the efficiency of heat exchangers and heat pumps. At 360 m (north-south) by 280 m (east-west) by 152-m-deep, borefield 4 has approximately 15.4 million m^3 of fill, surface sediments, and rock to offer thermal exchange capacity. The addition of the borefield 4 allowed better energy distribution and permitted the cooling of the other fields. However, it was well recognized that this problem cannot be sustainably addressed by merely adding new fields to dump heat. Thus, borefield 4 has been monitored continually in recognition of the long-term impact of its significance for handling for campus loads. Borefield 4 is instrumented with temperature monitoring wells (TMWs) (Figure 2) with fiber-optic loops down to the base. The red circles in the figure are the sentry wells drilled in the center of a section bounded by four GHX boreholes and are equipped with fiber loops grouted in direct contact with the ground. The blue squares show the piezometric wells in the field, which are also equipped with fiber optic loops, in addition to being equipped with a piezometer screen in a shallow aquifer and a piezometer screened in a deep aquifer.

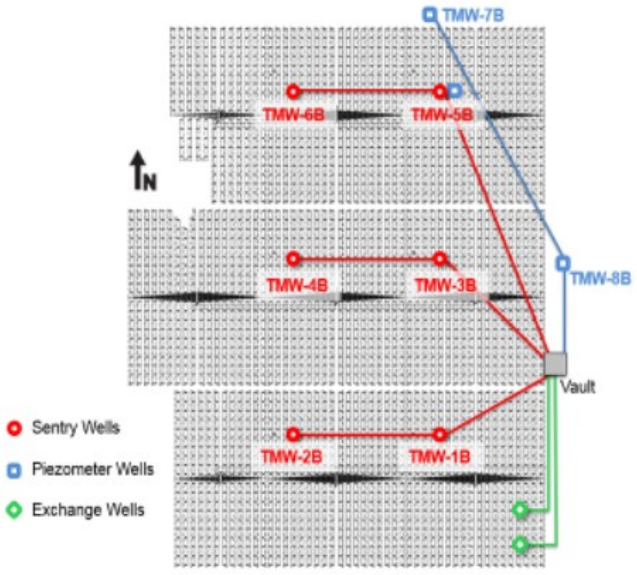

Figure 2: Design for borefield 4 with distributed temperature array to monitor temperatures (after McDaniel et al. 2018b).

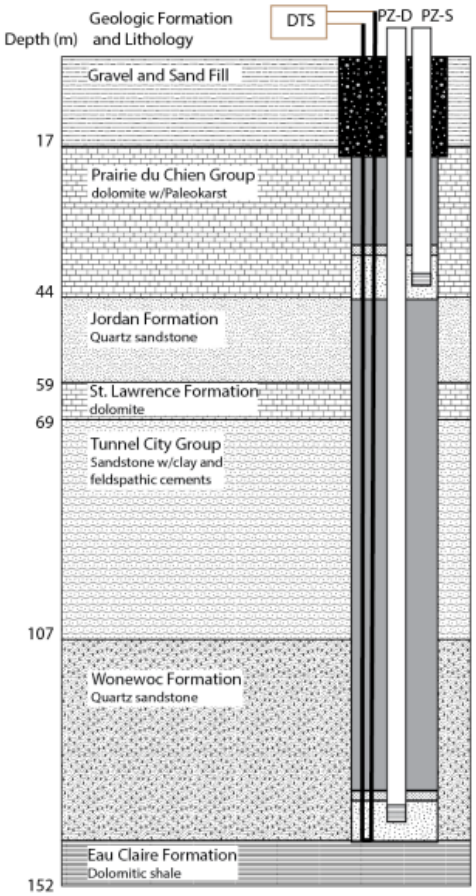

Figure 3: Borefield 4 geologic profile (Hart et al. 2022).

The geologic profile of borefield 4 (Figure 3) starts with a 10-m layer of gravel and sand fill at the surface, and the first bedrock encountered at borefield 4 is the Oneota Dolomite formation of the Prairie du Chien group. This formation is characterized by the presence of chertz nodules, oolites, and predominantly hard dolomite. The next 10 m are the clean quartzose sandstones of the Jordan formation. Beneath the Jordan formation sits the St. Lawrence formation. The next 35 m are characterized as the Tunnel City Formation, a sandstone stratum with clay and feldspathic cement binding together the sand particles. These cements conduct heat at a much lower rate than quartz and lower the overall thermal conductivity of the Tunnel City Formation. Underlying the Tunnel City is the Wonewoc sandstone, this layer is composed primarily of clean quartz-rich sandstone. At the bottom of borefield 4 lies the Eau Claire Formation, a dolomitic, fossiliferous, and glauconitic shale layer. The Eau Claire Formation has the lowest thermal conductivity of any unit at borefield 4 (McDaniel et. al 2018a; Thomas 2019).

2.2 Instrumentation

The thermal instrumentation system includes an interrogator with a photodiode to generate light pulses and measure the amplitudes of the Stokes and anti-Stokes Raman backscatter, fiber-optic cables, connectors, water baths, and thermistors. A Sensornet Sentinel DTS-LR interrogator with a 16-channel multiplexor (Figure 4) was placed in a 10 m by 10 m by 5 m subsurface vault on the east side of the borefield. It provides up to 0.01-°C temperature resolution, 1-m spatial resolution for over 10 km of fiber (Sensornet 2015). Fiber-optic cables are multi-mode 50/125 µm OM2 ClearCurve Plenum Orange, 2-mm outer diameter. All fibers are protected with 6.35-mm-diameter HDPE plastic piping to avoid differential stress or pinching in the fiber which would result in signal loss. Two PT100 Platinum Thermistors (±0.25 °C) are connected directly to the Sentinel interrogator to collect continuous calibration bath temperatures and pair it to the appropriate fiber data. Temperatures were calibrated by a dynamic, double-ended, centralized, and remotely accessible manual routine.

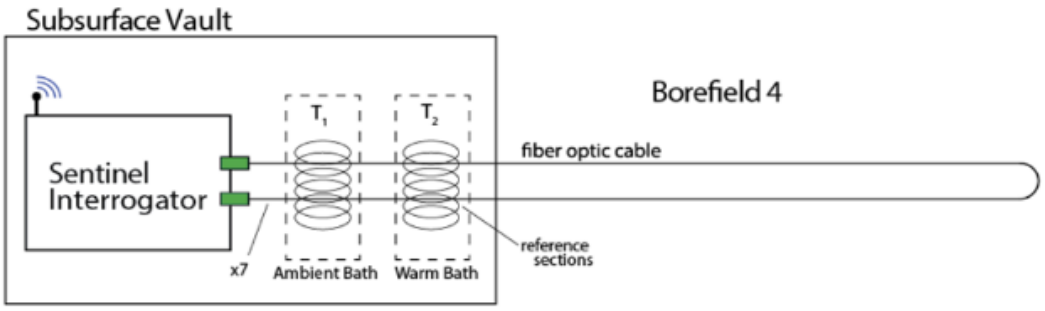

Figure 4: Schematic of double-ended, dynamic, centralized calibration setup in the vault (McDaniel et al. 2018b)

3. CALIBRATION METHODOLOGY AND DATA ANALYTICS

A double-ended, manual, centralized, dynamic, and remotely accessible calibration was developed with cold and hot water baths. The calibration equipment and baths were centrally placed in a vault to easy access, as shown in Figure 4. The cold bath was placed in a refrigerator, and a submersible circulation pump provided heat for the hot bath. Both baths had small pumps to maintain a uniform temperature throughout and prevent thermal stratification. Each of the seven fiber loops has a coil in both the cold and the hot baths, is buried in communication trenches until reaching the sentry wells, returns in trenches, and again has a coil in both baths. Dynamic calibration was chosen when a static calibration was first analyzed and a temperature drift of over 0.5 °C was observed in only the first week of data collection. Double-ended configuration was chosen over single-ended for the ability to calculate local differential attenuation ($\Delta\alpha$) independently of calibration at any fiber section (Δz) desired by comparing the forward ($\Rightarrow$) and reverse ($\Leftarrow$) Raman spectra data. During alternative measurement periods, the pulses are sent into the fiber from one end (forward) and then from the other end (reverse). If a small reference section of the cable remains a constant temperature, Equation 2 (van de Giesen et al. 2012) can be used to solve for differential attenuation, $\Delta\alpha$.

$$\int_{z}^{z+dz} \Delta\alpha\, z'(dz') = \frac{\ln\frac{P_S(z+\Delta z)}{P_{AS}(z+\Delta z)_{\Rightarrow}} - \ln\frac{P_S(z)}{P_{AS}(z)_{\Rightarrow}} + \ln\frac{P_S(z+\Delta z)}{P_{AS}(z+\Delta z)_{\Leftarrow}} - \ln\frac{P_S(z)}{P_{AS}(z)_{\Leftarrow}}}{2} \quad (2)$$

We use two baths in each loop to provide an over-determined system of equations. Δz equal to the 1-m spatial resolution was used and subsequently, local differential attenuations were optimized on a single cable between splices by the piecewise method described in van de Giesen et al. (2012). We recalculate $\Delta\alpha$ with each data trace to allow cable $\Delta\alpha$ values to vary over time. Once $\Delta\alpha$ is determined for each section of the fiber, we use a piecewise function to combine the results determined for each section of fiber. Then the log power ratios and $\Delta\alpha$ are determined at each bath, as they are used to determine constants γ and C. The constant values of γ and C are substituted into Equation (1) to determine temperature down the length of the cable. To allow for smoother plots, with less fluctuation in temperature between time steps, we average the γ values across the fiber length. This fixed γ value is then used to let the constant C be variable through the cable. Finally, we calculate the temperatures by putting the constants in equation (1).

Double-ended routines provide us with both forward and reverse Raman spectra data in both up and down directions in the well. Hence, we get four calibrated temperature values for one location on the fiber, two from forward and reverse signals, and two for the fiber going down in the well and coming up. We average all these values to get a more reliable temperature calculation, starting by averaging the temperatures obtained from forward and reverse signals. When the spatial-temporal temperature data were collected, we analyzed the results using visualization techniques in Python. We implement packages like Pandas, Numpy, Matplotlib to visualize color floods of temperatures over the years and graphs to analyze the Stokes and anti-Stokes signals, bath temperatures, and variation in the field temperatures.

4. RESULTS AND DISCUSSION

FO-DTS system was used to monitor the borefield 4 of the district-scale GSHP system, and data ware calibrated dynamically to obtain the temperature profiles as discussed in Section 3. As a part of that calibration method, we apply an overall average γ value to all the data for every month, and a variable C is used. The color floods provided insights about the temporal and spatial variation of the temperature and significant conclusions were made using the same data. Eight temperature monitoring wells (TMWs) were under study for over 6 years (continuing still) starting from 2015, like the one shown in Figure 5. TMW1B (Figure 5) provides us with the temperature profile for one of the monitoring wells over the years. The white portion is the missing data due to issues with the system and our inability to correct it due to the pandemic period. Figure 5 shows drastic surface temperature changes compared to the more stable ground temperatures. These results also support the hypothesis of heterogeneous heat transfer and the impact of water flow (close to 30 m depth) on the heterogeneous heat transfer. Over the years, seasonal trends can be observed in the ground temperatures.

Additionally, a notable overall temperature increase can be observed within the past two years. To get better insights, temperatures were plotted at selected depths shown in Figure 6. An increase of approximately 0.5 °C can be seen when we compared the peaks in 2016 and 2022, potentially due to dominating cooling loads and relatively more heat dumped. This does not just impact the system performance negatively but is also an environmental concern as the environmental effects of increasing groundwater temperatures remain relatively unknown.

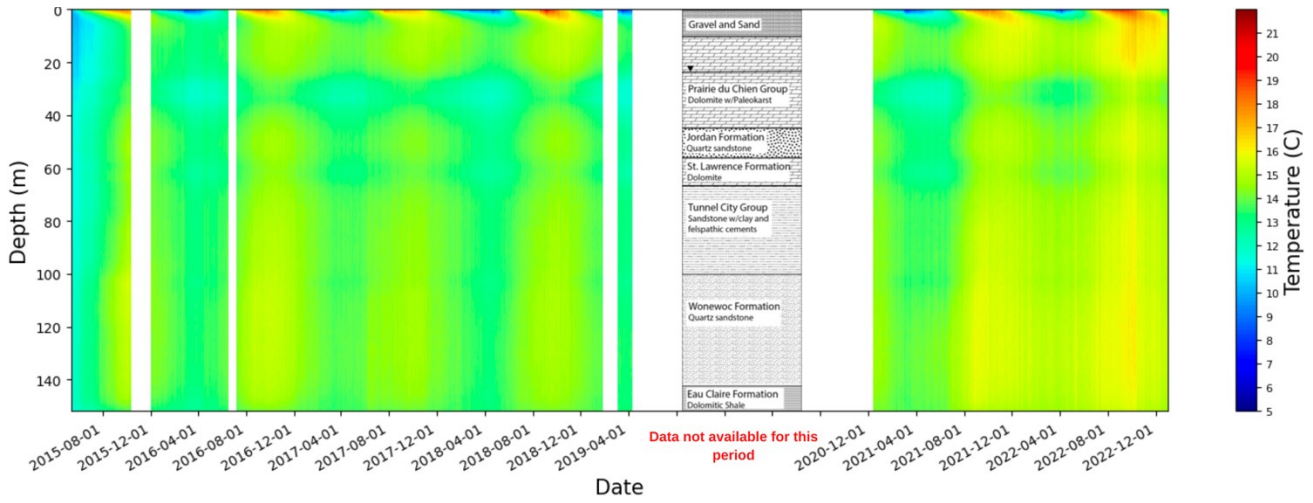

Figure 5: Temperature profile for temperature monitoring well (TMW) 1 with borefield 4 geologic profile.

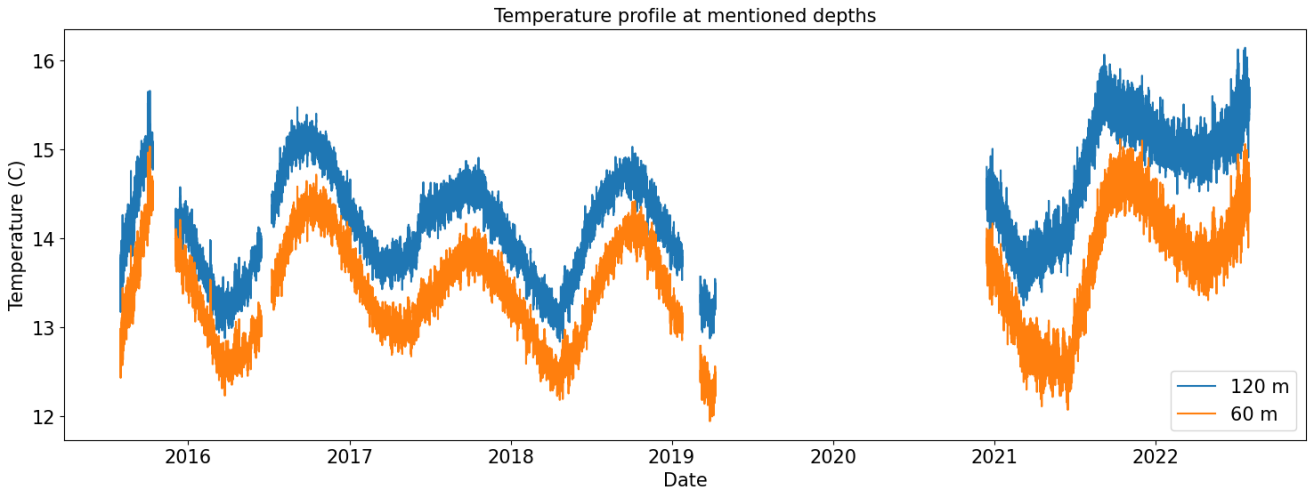

Figure 6: Temperature profiles at 60 m and 120 m below the ground surface for TMW 1.

While these temperature profiles give us a fair idea of the borefield behavior over the years, there are still some errors in the data. Further analyses were done for December 2022, to explore the potential cause of this error. First, the variation in the four calibrated temperatures obtained from forward and reverse signals and the fiber going down in the well and coming up were studied. Figure 7 shows how these values vary for the first reading for December with the depth of the well. While the variation at some depths is as high as 0.5 °C, it is typically less than 0.3 °C. This variation is one of the potential reasons shown by the streaks seen in the color floods. While errors can be either instrumentation, calibration, or random, we are mostly concerned about the possible errors in calibration and instrumentation. Taking the average makes the measurements more reliable, which is why the double-ended calibration was used.

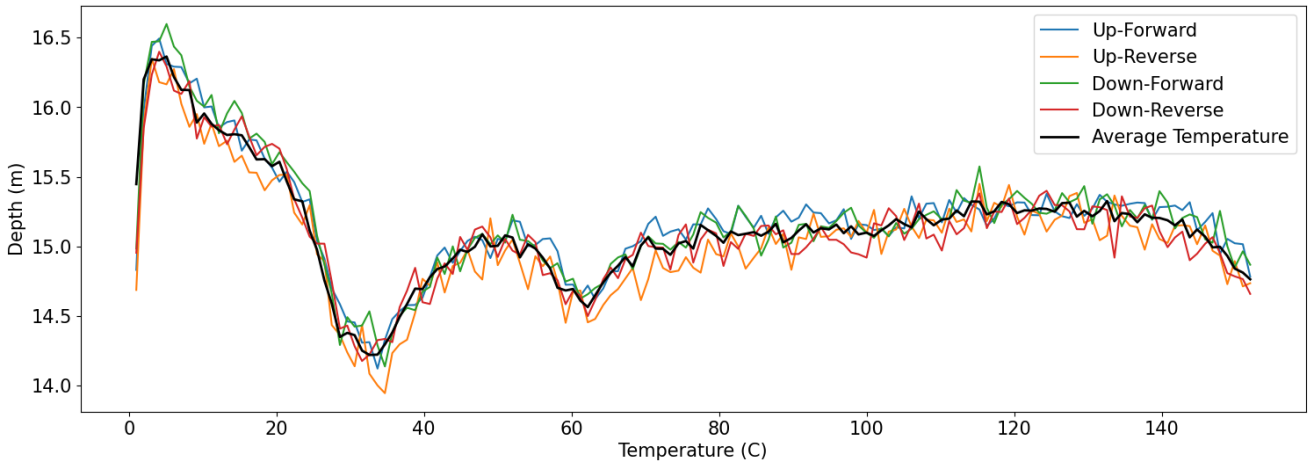

Figure 7: Calibrated temperatures from forward and reverse Stokes signals, and for fiber going down well and back up.

The temperatures of the calibration baths were observed as shown in Figures 8 through 10. Figure 8 shows the variation of the borefield 4 temperatures at 60 m and 120 m below the ground with the cold bath temperatures. Note that the values were plotted after adding 10 °C to the original measured bath temperatures to map the variation in bath temperatures better in the graph. Similarly, the bath temperatures in Figures 9 and 10 are also scaled as labeled in the graphs. Figure 9 shows the borefield 4 temperatures at the same depths as mentioned above for December 2022 with the difference in the hot and cold bath temperatures. While there is a considerable variation in the bath temperature measurements, there is no consistent mapping of the variation to the calibrated temperatures. Although we hypothesized that there is a contribution of these varied bath temperatures measured which needs to be further examined to correct/minimize it. These observations still do not give us an apparent reason for the streaks observed in the color floods.

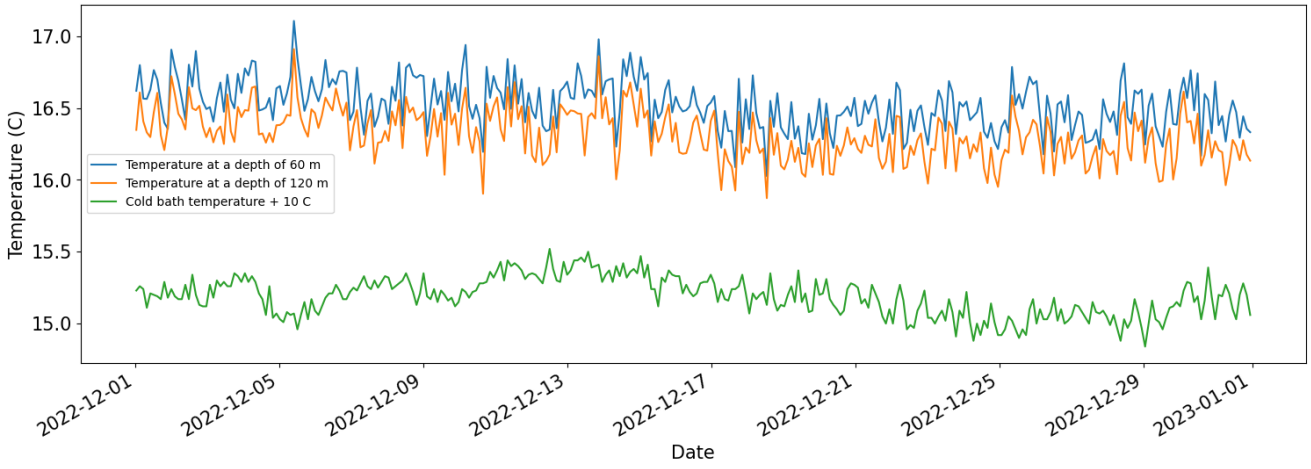

Figure 8: Cold bath temperatures (+10 ºC) and temperature variation at depths of 60 and 120 m below the ground surface for December 2022.

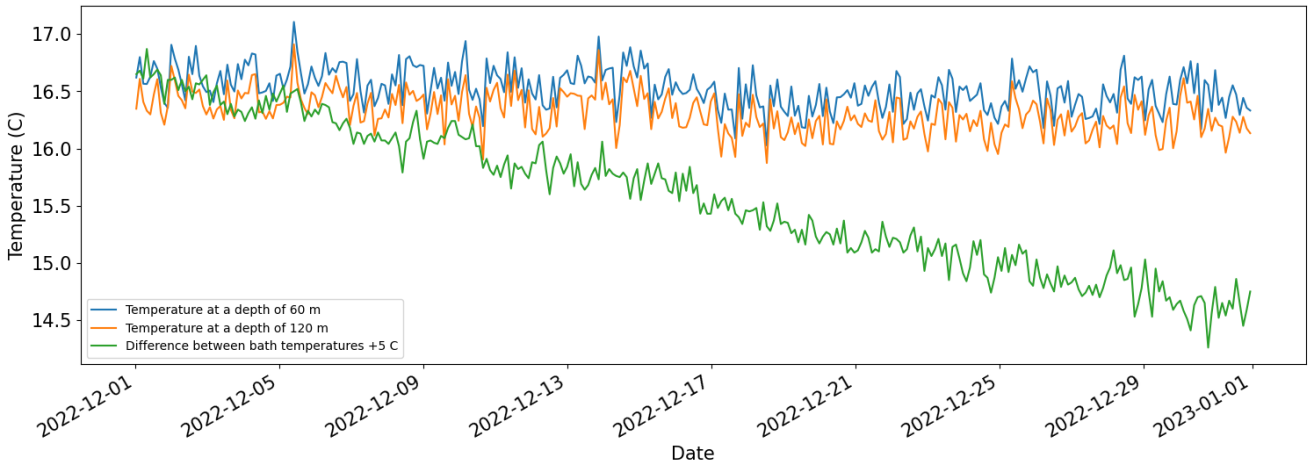

Figure 9: Difference in cold and hot bath temperatures (+5 ºC) and temperature variation at depths of 60 and 120 m below the ground surface for December 2022

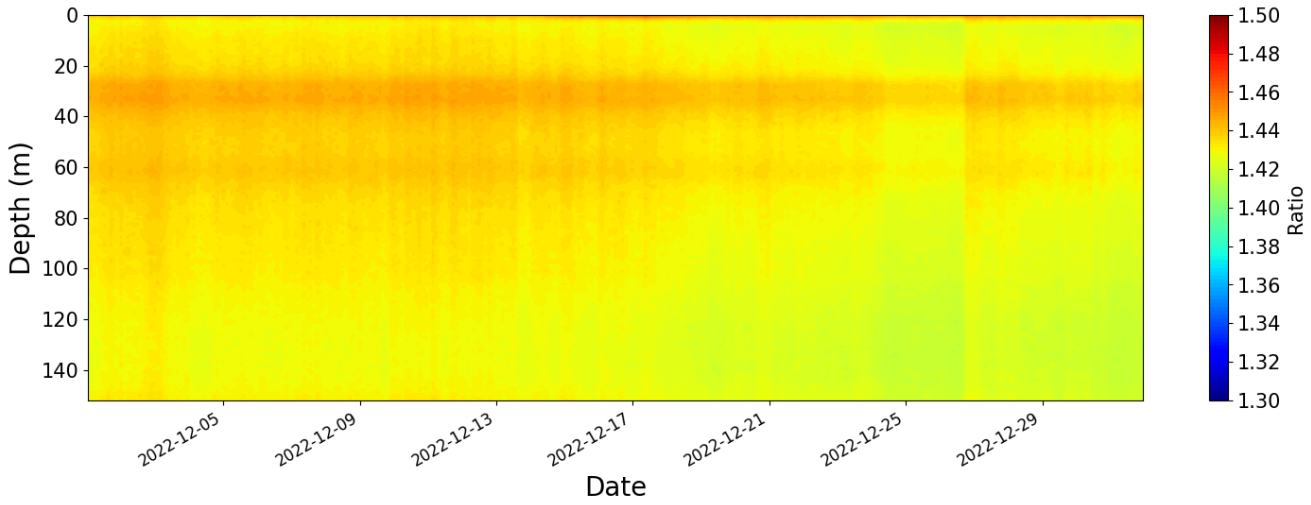

Figure 10: Variation of the ratio of Stokes to anti-Stokes (Up) signals during December 2022

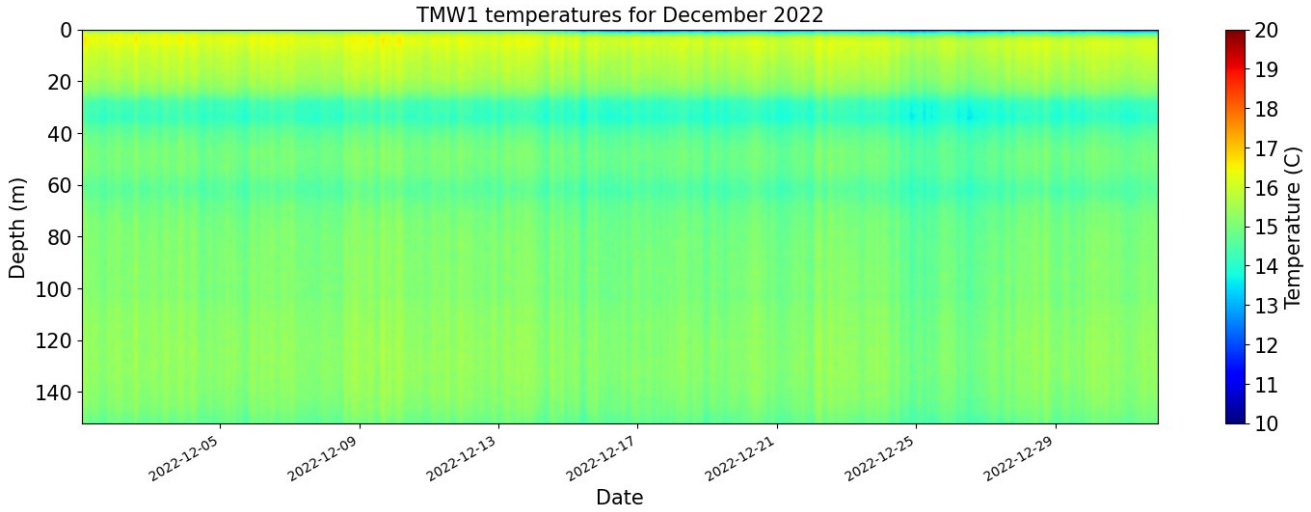

Figure 11: Temperature variation for TMW1 during December 2022.

Finally, we studied the Stokes and anti-Stokes signals over one month period. Figure 10 documents the ratio of the forward Stokes to Anti-Stokes signal for December 2022. There is a conspicuous change in the ratio at every time step (2 hours and 20 minutes), which can also be observed in the calibrated temperatures (plotted in Figure 11). This sudden change is potentially mapping to the streaks in the final temperature values for the wells. Unfortunately, the reason for the same is not coherent, whether this is an instrumentation error or a human error while setting up the instruments or collecting the signal values.

Figure 12 shows the changes in subsequent well temperatures for every time step for December in 2022. This means the y-axis represents the difference between the temperature at a particular time and the temperature one time step before that. The variation is as high as 0.5 ^{o}C at every 140-minute measurement at a depth of 120 m, which is not justified for consistent subsurface temperatures. Furthermore, this variation can be seen at different depths and is in fact, correlated. For example, Figure 13 shows the correlation between the change in subsequent temperatures at depths of 60 and 120 m. The R^2 value of 0.8126 means almost 81% correlation between the temperature differences at the two depths.

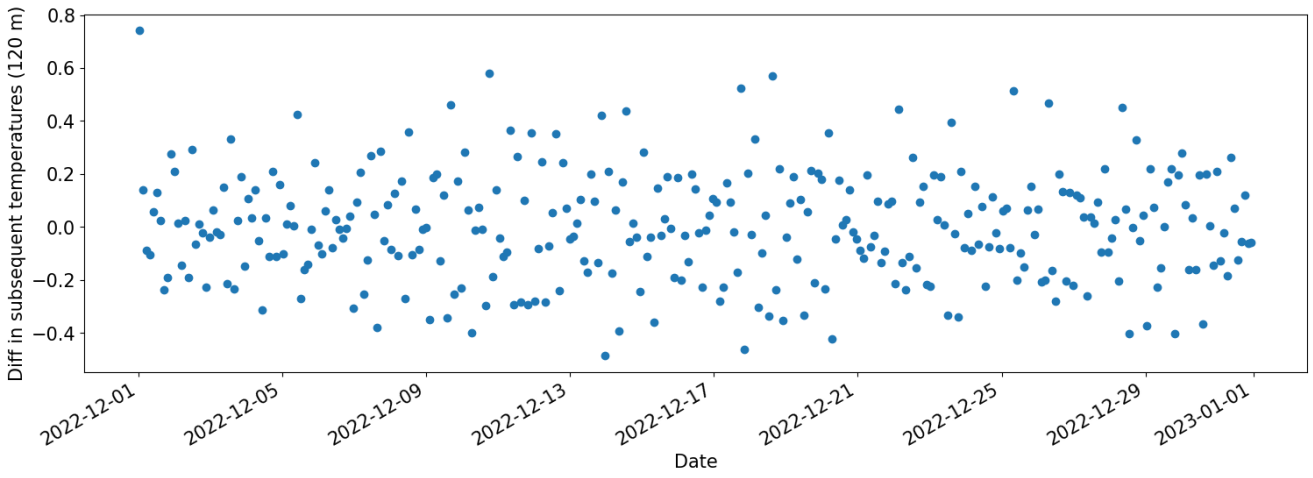

Figure 12: Variation in the well temperatures for every time step compared to the temperature one time step before at a depth of 120 m during December 2022.

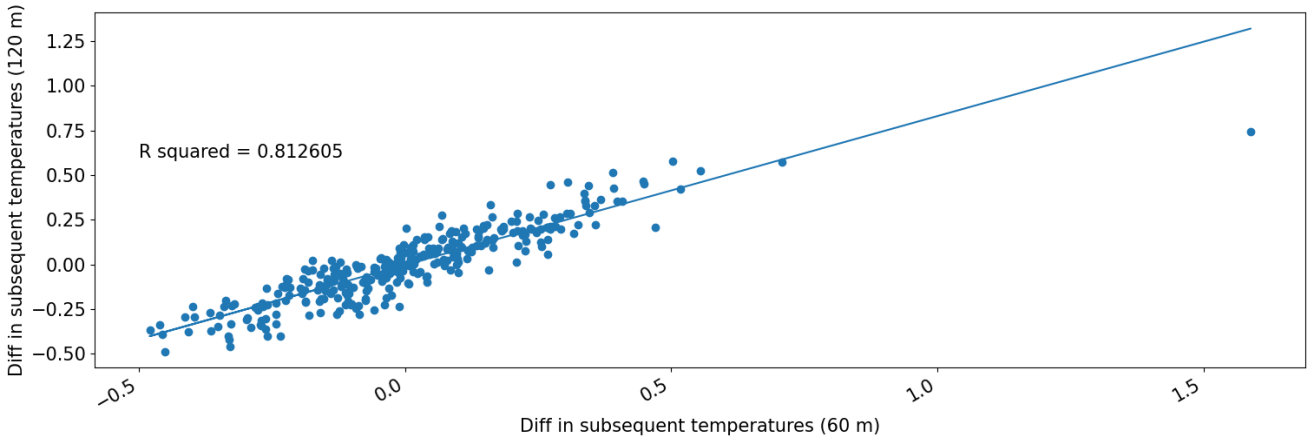

Figure 13: Variation in the well temperatures for every time step compared to the temperature 1-time step before at a depth of 120 m vs. 60 m.

5. CONCLUSION AND FUTURE SCOPE

Long-term data analysis of the temperature profiles for a geothermal exchange field showed a gradual increase in the borefield temperatures due to cooling-dominated loads. This trend concerns both system performance and the area's geology in the longer term. This can be addressed by designing the system according to the heterogeneous heat transfer in the borefields. These temperatures can further be used to calculate the net heat transfer into/from the field for specified periods and metrics like energy payback period and life cycle costs can be evaluated more precisely (Tinjum et al. 2023). Two potential reasons for the errors/variation were discussed in the paper. First, the noise in the bath temperatures can propagate to the calibrated values. Second, as discussed, the raw data of the signals collected might be the primary reason for the noise/streaks in the temperature profiles. The reasons for those noise/streaks and the amount

of noise propagated by both are yet to be known and need further analysis. Interpolation can be used to fill up the missing data for two years. Further, temporal data analytics can be leveraged to predict the future temperature profile. Steps can be taken on time to address the potential problems, like the increase in subsurface temperatures. For long-term DTS measurement systems, we strongly suggest regular checking on the instrumentation (connections, baths etc.), at least every six months to address any unexpected changes or malfunctions. We hope that the data and analysis provided in this paper may be used to develop more efficient design approaches, create better energy balance assessments, and calibrate long-term ground temperature change models.

ACKNOWLEDGEMENT

The authors would like to acknowledge Epic Systems Corporation for their generous contributions of time, talent, and resources in the ongoing development of this research. The Morse Company, General Heating and Air Conditioning Inc., Salas O'Brien (formerly MEP Associates), JP Cullen, and Teel Plastics all donated time, materials, and/or expertise, without which, this research would not have been possible. We acknowledge the National Science Foundation for sponsoring undergraduate research opportunities during the early phases of this project under Award # 1156674. We thank Mr. Adam McDaniel (Westwood Professional Services) for preparing the initial Matlab scripts to process and calibrate FO DTS data. Any opinions, findings, and conclusions or recommendations expressed in this material are those of the authors and do not necessarily reflect the views of the funding organizations.

REFERENCES

ASHRAE (2011)."Geothermal Energy." In 2011 ASHRAE Handbook - HVAC Applications." Ch. 34. American Society of Heating, Refrigerating and Air-Conditioning Engineers.

Bloom, E. and Tinjum, J. (2016). "Fully Instrumented Life-cycle Analyses for a Residential Geo-exchange System." Geo-Chicago 2016, 114-124.

des Tombe, B., Schilperoort, B., and Bakker, M. (2020). "Estimation of Temperature and Associated Uncertainty from Fiber-Optic Raman-Spectrum Distributed Temperature Sensing." Sensors, 20, 2235.

Hart, D. J., Tinjum, J. M., Fratta, D., Thomas, L. K., and Carew, E. L. (2022). "Radiators or Reservoirs: Heat Budgets in District-Scale Ground-Source Geothermal Exchange Fields." 47th Workshop on Geothermal Reservoir Engineering. Stanford University, Stanford, California, February 7–9, 2022. SGP-TR-223.

Hausner, M. B., Suárez, F., Glander, K. E., van de Giesen, N., and Selker, J.S., and Tyler, S. W. (2011). "Calibrating Single-Ended Fiber-Optic Raman Spectra Distributed Temperature Sensing Data." Sensors. 11.

McDaniel, A., Tinjum, J. M., Hart, D. J., and Fratta, D. (2018b). "Dynamic Calibration for Permanent Distributed Temperature Sensing Networks." IEEE Sensors Journal, 18(6).

McDaniel. A., Fratta, D., Tinjum, J., and Hart, D. (2018a). "Long-term District-scale Geothermal Exchange Borefield Monitoring with Fiber Optic Distributed Temperature Sensing." Geothermics. 72C, 193–204.

Reddy, K. R., Ghimire, S.N., Wemeyi, E., Zanjani, R., and Zhao, L. (2020). "Life Cycle Sustainability Assessment of Geothermal Heating and Cooling System: UIC case study." ICEGT 2020 E3S Web of Conferences 205, 07003.

Selker, J. S., Thevenaz, L., Huwald, H., Mallet, A., Luxemburg, W., van de Giesen, N., Stejskal, M., Zeman, J., Westhoff, M., and Parlange, M. B. (2006). "Distributed Fiber-optic Temperature Sensing for Hydrologic Systems." Water Resource Res., 42, W12202, doi:10.1029/2006WR005326.

Sensornet (2015). "Sentinel DTS User Manual." Sensornet Ltd., Hertfordshire, U.K.

Suárez, F., Aravena, J. E., Hausner, M. B., Childress, A. E., and Tyler, S. W. (2011). "Assessment of a Vertical High-resolution Distributed-temperature-sensing System in a Shallow Thermohaline Environment." Hydrol. Earth Syst. Sci., 15, 1081-1093.

Tinjum, J. M., Yilmaz, M., Heeg, E., Fratta, D., Hart, D. J., and Attri, S. D. (2023). "Energy Efficiency and Life Cycle Assessment of a District-Scale Geothermal Exchange Field." 48th Workshop on Geothermal Reservoir Engineering. Stanford University, Stanford, California, February 6–8, 2023. SGP-TR-224.

Thomas, L. K. (2019). "District-Scale Geothermal System Performance Evaluation using Thermodynamic and Environmental Analysis." MS Thesis. University of Wisconsin-Madison.

van de Giesen, N., Steele-Dunne, S. C., Jansen, J., Hoes, O, Hausner, M. B., Tyler, S., and Selker, J. (2012). "Double-Ended Calibration of Fiber-Optic Raman Spectra Distributed Temperature Sensing Data." Sensors, 12, 5471-5485.